A three-dimensional study of a crustal low velocity region beneath the 9°03′N overlapping spreading center

S. Bazin,[1] A. J. Harding, G. M. Kent, and J. A. Orcutt

Cecil and Ida Green Institute of Geophysics and Planetary Physics, University of California San Diego, USA

S. C. Singh,[1] C. H. Tong,[2] J. W. Pye, P. J. Barton, M. C. Sinha,[3] R. S. White, and R. W. Hobbs

Bullard Laboratories, Department of Earth Sciences, University of Cambridge, UK

H. J. A. Van Avendonk

University of Texas Institute for Geophysics, Austin, USA

[1]   Overlapping spreading centers (OSCs) play a key role in models of magma distribution at fast spreading ridges. To investigate the relationship between ridge-axis discontinuities and magma supply, we conducted a three-dimensional seismic reflection and tomography experiment at the 9°03′N OSC along the East Pacific Rise. Tomographic analysis imaged a broad mid-crustal low velocity zone (LVZ) beneath parts of the overlapper and the associated overlap basin, demonstrating that it is magmatically robust. The complementary datasets reveal a complex storage and tapping of melt: the LVZ and melt sill at either end of the overlap basin are not simply centered beneath the rise crest but are skewed inwards. The subsequent focussing of the LVZ and sill beneath the axis of the eastern limb appears to be due to melt migration toward the tip. The OSC western limb is less magmatically robust and may be in the process of dying.   *INDEX TERMS:* 3035 Marine Geology and Geophysics: Midocean ridge processes; 3025 Marine Geology and Geophysics: Marine seismics (0935); 7220 Seismology: Oceanic crust. **Citation:** Bazin, S., et al., A three-dimensional study of a crustal low velocity region beneath the 9°03′N overlapping spreading center, *Geophys. Res. Lett.*, *30*(2), 1039, doi:10.1029/2002GL015137, 2003.

1.   Introduction

[2]   Between major transform faults (TF), the fast spreading East Pacific Rise (EPR) is offset by small discontinuities in which two sections of the ridge overlap significantly [*Macdonald et al.*, 1991]. Interpretation of these features varies, depending upon the assumed crustal accretion model for the EPR. In one model, the supply of magma is essentially two-dimensional with the crustal magma chamber being locally fed along an entire ridge segment. Perhaps, there is some along-axis focussing of the magma supply, which is reflected in the finer scale segmentation of the ridge [10–20 km scale; *Dunn et al.*, 2000]. In an alternative model, mantle upwelling is highly focussed into mantle diapirs with a single diapir supplying melt to ridge segments between major discontinuities. This model presents OSCs as magmatically starved regions of the ridge axis far from the upwelling diapirs, where the limbs are underlain by small and intermittent magma chambers [*Macdonald et al.*, 1984]. The ARAD (Anatomy of a Ridge Axis Discontinuity) active-source seismic survey was undertaken at 9°N along the EPR to investigate the local melt delivery of an OSC. The experiment was designed to examine whether magma was remotely or locally supplied and whether each limb of the OSC has its own melt supply or share a single supply. A combined three-dimensional reflection/refraction seismic survey such as ARAD is needed to provide the data necessary to image the internal structure of an OSC and the pathways of melt from the mantle to the seafloor.

2.   Geologic Setting

[3]   A combination of various seismic experiments carried out along the 9°–10°N segment has led to the definition of the present structural model for the axial magma chamber at fast-spreading mid-ocean ridges [e.g., *Kent et al.*, 1990; *Sinton and Detrick*, 1992; *Crawford and Webb*, 2002; *Dunn et al.*, 2000]. A thin, narrow, lens-like melt reservoir (50–300 m thick, ~1 km wide) is nearly continuous along the axis of the segment [*Detrick et al.*, 1987; *Kent et al.*, 1990, 1993]. A broader LVZ underlies the melt lens and is believed to be a region of hot material and possibly molten rocks [*Harding et al.*, 1989; *Vera et al.*, 1990]. Negative velocity anomalies as large as −0.5 to −2.7 km/s have been reported in the axial LVZ [*Toomey et al.*, 1990; *Dunn et al.*, 2000] and extend 3 to 10 km off axis.

[4]   The right-stepping 9°03′N OSC is the largest topographic disruption along the 9°N segment; it offsets the ridge axis by 8 km (Figure 1). A sparsely spaced set of multichannel seismic (MCS) profiles shows distinct jumps in the axial melt widths at small ridge offsets [*Kent et al.*, 1993]. Deeper tomographic results image a continuous channel of mantle partial melt beneath the 9°03′N OSC which does not support the model of a single point of upwelling. Therefore OSCs are not necessarily associated with a discontinuity in melt supply [*Dunn et al.*, 2001] but are probably initiated by changes in local spreading direction [e.g., *Lonsdale*, 1983]. However, the crustal melt delivery to the OSC is still unresolved.

---

3. 3-D Tomographic Inversions

[5] The observation of geometric shadow zones along seismic refraction lines crossing the OSC (Figure 2) is indicative of a mid-crustal LVZ. The seismic arrivals that traveled at depth beneath the OSC basin are delayed and attenuated, resulting in a reduced signal-to-noise ratio and reduced apparent trace-to-trace coherence in the data. We infer the LVZ to be a region of elevated temperature and possibly partially molten rock beneath the ridge-axis discontinuity. We performed a 3D-tomographic analysis [*Van Avendonk et al.*, 1998] of over 20,000 Pg and PmP arrivals to assess the extent and the structure of the LVZ. The shots came from 11 refraction lines (28 to 72-km long) and a subset of the 201 densely spaced MCS profiles. Further details of the experimental procedure are presented in *Bazin et al.* [2001]. Crustal thickness estimates will be presented elsewhere.

[6] We start the tomographic inversion with a one-dimensional model derived by forward modeling; no LVZ is explicitly built into it. The starting RMS travel-time residual is 121 ms and is reduced to 25 ms after 15 iterations (normalized variance reduction of 96%). Nominally this slightly underfits the data, as the total predicted RMS errors, which includes errors from bathymetry, travel-time picks, instrument and shot locations, instrument clock drift, and travel-time computation, is 17 ms. A superior data fit would be feasible if a weaker smoothing constraint was applied and finer grid cells were chosen.

[7] Sections of the 3-D velocity model solution mapped at mid-crustal depths are displayed in Figure 3. At 2.3 km depth, a LVZ is present beneath both the western and eastern
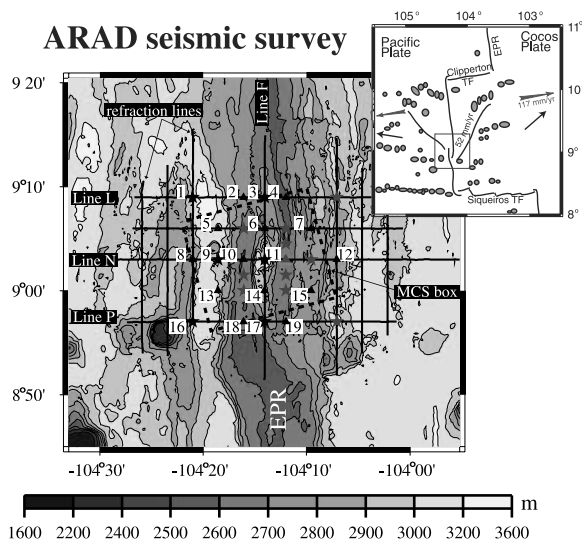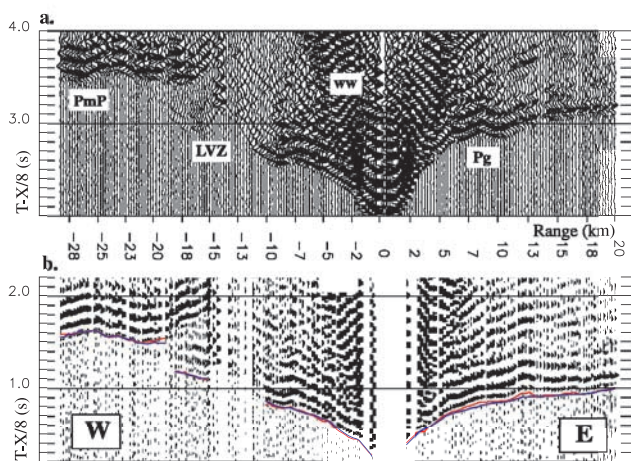

Figure 2. Representative data section recorded at site 12 along shotline N and illustrating the axial LVZ. A band-pass filter was applied for display purposes. (a) arrivals from the water waves (ww), from P waves refracting in the crust (Pg) and from P waves reflecting along the Moho discontinuity (PmP). The shadow zone between −10 and −20 km range suggests the presence of a LVZ. (b) a static topographic correction was applied to highlight the time delay (∼0.4 s) caused by the LVZ. The data picks are in red while the calculated travel times are in blue.

limbs, but does not cover the entire OSC; the western ridge tip north of 9°02′N does not manifest any LVZ. The low velocity anomalies are not simply centered beneath the two rise crests but are skewed inwards. The map at 3 km depth shows two zones of low velocities focused at the two extremities of the overlap basin. The northern portion of the LVZ is stronger and more deeply rooted. Resolution tests (Two resolution tests are presented as auxiliary material. The first test demonstrates that our method would be capable of recovering narrow LVZs beneath each limb. The second demonstrates that the inversion would not artificially fragment a single LVZ body beneath the basin into separate LVZ domains. The lack of low velocity body observed at the western ridge tip is not an artifact of the geometry. The tests demonstrate that the abrupt truncation of the LVZ north of 9°09′N (Line L) and south of 8°57′N (Line P) in Figure 3 is an artifact of the ray coverage.)[1] demonstrate that the experimental geometry and tomographic inversion are capable of recovering a structure similar to that observed.

4. Interpretation and Discussion

[8] Our results indicate the presence of a LVZ beneath the 9°03′N OSC. Neither a broad magma chamber spanning the entire overlap basin, nor distinct magma bodies centered beneath the two limbs, resides at mid-crustal depth. We report a velocity anomaly as low as −1 km/s, which is too big to be entirely due to temperature variations. Up to 57% of this anomaly can be explained by elastic velocity reduction due to elevated temperatures [*Christensen*, 1979] between a thermal reference [200°C, near axis temperature estimated

Figure 1. Bathymetric map of the 9°03′N OSC displaying refraction shot lines (black lines) and instrument locations (symbols). The 19 instruments used in the tomography inversion are numbered, triangles designate Scripps L-Cheapo hydrophones and stars designate Cambridge mini-DOBSs. The 2000 shots of the refraction experiment were fired every 110 s in order to minimize reverberative noise in the water column and ensure identification of weaker arrivals. The 201 MCS lines were shot in a 20 by 20 km box delineated with dashed lines. Inset shows the survey site relative to the 9°N segment and the OSC migration [*Carbotte and Macdonald*, 1992].
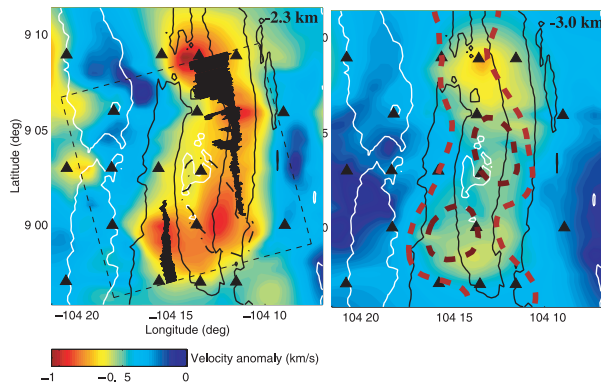
Figure 3. Map views of the LVZ 2.3 and 3.0 km below seafloor. The anomaly is calculated with respect to 6.8 km/s. Red/orange colors indicate slow velocity anomalies. The black in-fill shows the extent of the reflective melt lens detected by the MCS survey [dashed box; *Kent et al.*, 2000]. The low velocities at the propagating ridge tip observed 2.3 km bsfl, is not only an effect of the magma chamber, but results in part from a thick layer of slow extrusives [dash-dotted contoured area; *Bazin et al.*, 2001]. Superimposed orange and brown dash contours indicate mantle velocity anomalies (−0.4 and −0.5 km/s) observed at a depth of 7 km [*Dunn et al.*, 2001]. Bathymetric contours are overlain for reference; black and white contours are the 2700 and 3000-m isobaths. Triangles show the locations of ocean-bottom instruments.

with *Henstock et al.*, 1993] and the liquidus [1195°C, axial temperature maxima calculated with mean MgO; *Sinton and Detrick*, 1992]. Anelastic effects above solidus can increase the temperature derivative of seismic velocity [*Karato*, 1993]. These are not taken into account in our calculation as compositional variations (difficult to estimate and commonly neglected) would have even more effect on velocity [*Maclennan*, 2002]. The remaining velocity anomaly (43%) suggests the presence of partial melt in the crust but the aspect ratio of the melt pockets affects the velocity reduction: thin films lower the compressional velocity considerably more than tubules of melt [e.g., *Faul et al.*, 1994]. We predict melt amounts ranging from 3% (film geometry) to 12% (tubules), however our resolution tests[1] indicate that our tomographic method probably underestimates the amplitude of the anomaly.

[9] We compare the lateral extent of the axial LVZ with the melt lens reflections picked in the 3D reflectivity volume [*Kent et al.*, 2000]. The MCS survey reveals that two melt sills underlies both limbs and the northern part of the overlap basin. The eastern melt sill is unusually wide (up to 4 km) and shifted toward the west, while the western melt sill is of more typical width (∼1 km) [*Kent et al.*, 2000]. The eastern velocity anomaly shows the strongest amplitude (−1 km/s) beneath the widest part of the melt lens and diminishes toward the south. As the eastern melt sill narrows to 1 km width at 9°07′N, the LVZ becomes realigned with the topographic high. The eastern melt lens and LVZ vanish at 9°01′N but another lens starts to appear beneath the western limb. The depths computed by vertical integration of two-way travel-times through our velocity model show that the melt sills lie on average 1.7 km bsfl and that the eastern melt sill reflector deepens toward the south by ∼600 m along its 10 km-long narrow portion.

[10] Lava samples dredged from the eastern limb of the OSC show greater compositional diversity than those recovered from the western limb or from the adjoining southern and northern ridge axis : N-, E-, T-type lavas and even dacite composition were observed [Figure 4; *Langmuir et al.*, 1986; *Natland et al.*, 1986]. The high level of fractional crystallization observed in lavas from the eastern tip is likely a result of the diminishing size of the melt lens south of 9°07′N [e.g., *Sinton et al.*, 1983]. We suggest the following geometry for the magma supply of the propagating limb: melt arises from beneath the northern extremity of the overlap basin at 9°08′N and is trapped at the base of the dike complex. The lens channels melt upward and eastward toward the neovolcanic zone. Around 9°07′N, we observe a left lateral step of the low velocity region and a deep root to the LVZ is not imaged below this point. Therefore, we propose that melt feeding the eastern limb primarily emanates from vertical upwelling near 9°08′N. This deep supply is also suggested by the abundance of melt detected near Moho depths with a local peak in the axial compliance values at 9°08′N [*Crawford and Webb*, 2002]. Shallow melt migration toward the southern tip following mid-crustal fractures or cracks may be inferred from small en-echelon steps along the narrow section of the melt lens [Figure 4b of *Kent et al.*, 2000] and the evolved nature of the lavas due to
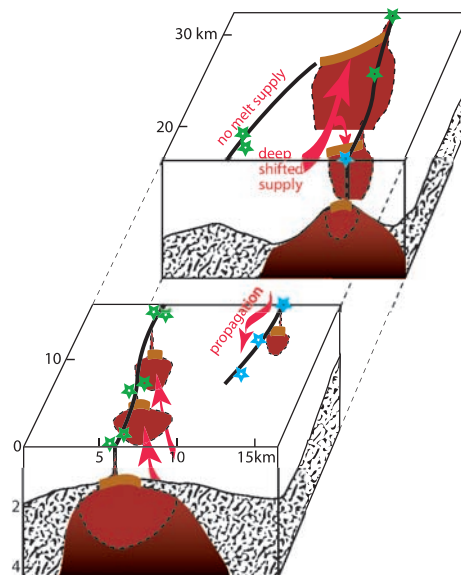

Figure 4. Simple possible model for the OSC crustal magma chamber based on wide-angle and reflection seismic results. The black lines indicate the ridge axis position: the white and stipple layers indicate inferred thickness of basalt and gabbro units (modified after *Macdonald et al.*, 1984). Seven colored sections are drawn to illustrate the variable shape of the continuous magma chamber along the ridge axis. The melt sill (orange lines) beneath the eastern limb is unusually wide and shifted on the side flanking the basin. An intense and deeply rooted low velocity body (red colors) underlies the northern half of the basin and probably feeds the eastern limb. The high level of fractionation on the eastern ridge (fractionated dredges shown as blue stars) imply a colder environment with small or intermittent magma bodies at the propagating tip. Normal MORB (green stars) and more typical magma chamber dimensions are found on the western limb.

longer residence time in the crust. This geometry is consistent with the long-term southward propagation of the eastern limb into older crust [*Carbotte and Macdonald*, 1992].

[11] The western limb has characteristics of a more typical EPR axis: relatively unevolved N-type basalts, average melt lens width, and both the LVZ and melt lens underlie the axial high although they are slightly displaced toward the OSC basin. The melt lens and the LVZ disappear north of 9°02′N indicating that the western limb may be in the process of dying or be quiescent as the eastern limb surges. In fact, a near-bottom photography revealed that the oldest pillow basalts are found at the western ridge tip north of 9°02′N [*Sempéré and Macdonald*, 1986].

[12] A recent mantle velocity study imaged a continuous channel of partial melt beneath the 9°03′N OSC with two local peaks at 9°00′ and 9°04′N [*Dunn et al.*, 2001]. Surprisingly, the two crustal LVZs observed here are not directly aligned with the underlying peaks of mantle supply (Figure 3). These snapshots taken at different depths can picture the complex trajectory of the melt from mantle depths to seafloor. Melt delivery seems to follow pathways created by weaker regions in the crust at either end of the OSC basin. In fact, *Pollard and Aydin* [1984] predicted intense mechanical interaction between OSC ridge tips where stresses are concentrated. We infer that the melt focusing observed at 9°08′N is not due to enhanced local mantle supply but to a more permeable crust.

5. Conclusions

[13] We have successfully applied 3-D seismic tomographic inversions to an extensive refraction data set at the 9°03′N OSC along the EPR. A low-velocity body underlies most of the axial discontinuity except beneath the western ridge tip. At shallow depth, the low velocity zone underlies the melt sill reflection. The LVZ is not centered below the two rise crests but is skewed toward the OSC basin.

[14] The amplitude of the eastern low velocity anomaly (at 9°08′N) and the large width of the melt lens suggests that the melt delivery is probably greater in the northern part of the OSC. The eastern melt sill deepens as it narrows toward the ridge tip. Fractionated lavas were found at this propagating ridge tip and are probably associated with the diminishing magma chamber. We postulate that melt arises from beneath the northern extremity of the overlap basin and is injected into the propagator.

[15] Rather than being fed by along axis flow from magmatically robust regions of the 9°N segment, the OSC is supplied by a local mantle source, which itself is misaligned compared to the neovolcanic zone.

References

Bazin, S., A. J. Harding, G. M. Kent, J. A. Orcutt, C. H. Tong, J. W. Pye, S. C. Singh, P. J. Barton, M. C. Sinha, R. S. White, R. W. Hobbs, and H. J. A. Van Avendonk, 3-D shallow crustal emplacement at the 9°03′N overlapping spreading center on the East Pacific Rise: Correlations between magnetization and tomographic imaging, *J. Geophys. Res.*, *106*, 16,101–16,117, 2001.

Carbotte, S., and K. Macdonald, East Pacific Rise 8°–10°30′N: Evolution of ridge segments and discontinuities from SeaMARC II and three-dimensional magnetic studies, *J. Geophys. Res.*, *97*, 6959–6982, 1992.

Christensen, N. I., Compressional wave velocities in rocks at high temperatures and pressures, critical thermal gradients, and crustal velocity zones, *J. Geophys. Res.*, *84*, 6849–6857, 1979.

Crawford, W. C., and S. C. Webb, Variations in the distribution of magma in the lower crust and at the Moho beneath the East Pacific Rise at 9°–10°N, *Earth Planet. Sci. Lett.*, *203*, 117–130, 2002.

Detrick, R. S., P. Buhl, E. Vera, J. Mutter, J. Orcutt, J. Madsen, and T. Brocher, Multi-channel seismic imaging of a crustal magma chamber along the East Pacific Rise, *Nature*, *326*, 35–42, 1987.

Dunn, R. A., D. R. Toomey, and S. C. Solomon, Three-dimensional seismic structure and physical properties of the crust and shallow mantle beneath the East Pacific Rise at 9°30′N, *J. Geophys. Res.*, *105*, 23,537–23,555, 2000.

Dunn, R. A., D. R. Toomey, R. S. Detrick, and W. S. D. Wilcock, Continuous mantle melt supply beneath an overlapping spreading center on the East Pacific Rise, *Science*, *291*, 1955–1958, 2001.

Faul, U. H., D. R. Toomey, and H. S. Waff, Intergranular basaltic melt is distributed in thin, elongated inclusions, *Geophys. Res. Lett.*, *21*, 29–32, 1994.

Harding, A. J., J. A. Orcutt, M. E. Kappus, E. E. Vera, J. C. Mutter, P. Buhl, R. Detrick, and T. Brocher, Structure of young oceanic crust at 13°N on the East Pacific Rise from ESPs, *J. Geophys. Res.*, *94*, 12,163–12,196, 1989.

Henstock, T. J., A. W. Woods, and R. S. White, The accretion of oceanic crust by episodic sill intrusion, *J. Geophys. Res.*, *98*, 4143–4161, 1993.

Karato, S., The importance of anelaticity in the interpretation of seismic tomography, *Geophys. Res. Lett.*, *20*, 1623–1626, 1993.

Kent, G. M., A. J. Harding, and J. A. Orcutt, Evidence for a smaller magma chamber beneath the East Pacific Rise at 9°03′N, *Nature*, *344*, 650–653, 1990.

Kent, G. M., A. J. Harding, and J. A. Orcutt, Distribution of magma beneath the East Pacific Rise near the 9°03′N overlapping spreading centre from forward modelling of CDP data, *J. Geophys. Res.*, *98*, 13,971–13,995, 1993.

Kent, G. M., S. C. Singh, A. J. Harding, M. C. Sinha, J. A. Orcutt, P. J. Barton, R. S. White, S. Bazin, R. W. Hobbs, C. H. Tong, and P. W. Pye, Evidence from three-dimensional seismic reflectivity images for enhanced melt supply beneath mid-ocean ridge discontinuities, *Nature*, *406*, 614–619, 2000.

Langmuir, C. H., J. F. Bender, and R. Batiza, Petrological and tectonic segmentation of the East Pacific Rise, 5°30′–14°30′N, *Nature*, *322*, 422–429, 1986.

Lonsdale, P., Overlapping rift zones at the 5.5°S offset of the East Pacific Rise, *J. Geophys. Res.*, *88*, 9393–9406, 1983.

Macdonald, K. C., J. C. Sempéré, and P. J. Fox, East Pacific Rise from Siqueiros to Orozco Fracture Zones: Along-strike continuity of axial neovolcanic zone and structure and evolution of overlapping spreading centre, *J. Geophys. Res.*, *89*, 6049–6069, 1984.

Macdonald, K. C., D. S. Scheirer, and S. M. Carbotte, Mid-ocean ridges: Discontinuities, segments and giant cracks, *Science*, *253*, 986–994, 1991.

Maclennan, J., The magmatic structure of mid-ocean ridges: Integrating geophysical and petrologic observations, *Lithos Science Report*, *4*, 81–90, 2002.

Natland, J., C. Langmuir, J. Bender, R. Batiza, and C. Hopson, Petrologic systematics in the vicinity of the 9°N non-transform offset, East Pacific Rise, *Eos Trans. AGU*, *67*, Fall Meet. Supp., 1986.

Pollard, D. D., and A. Aydin, Propagation and linkage of oceanic ridge segments, *J. Geophys. Res.*, *89*, 10,017–10,028, 1984.

Sempéré, J.-C., and K. C. Macdonald, Deep-Tow studies of the overlapping spreading centres at 9°03′N on the East Pacific Rise, *Tectonics*, *5*, 881–900, 1986.

Sinton, J. M., D. S. Wilson, D. M. Christie, R. N. Hey, and J. R. Delaney, Petrologic consequences of rift propagation on oceanic spreading ridges, *Earth Planet. Sci. Lett.*, *97*, 193–207, 1983.

Sinton, J. M., and R. S. Detrick, Mid-ocean ridge magma chambers, *J. Geophys. Res.*, *97*, 197–216, 1992.

Toomey, D. R., G. M. Purdy, S. C. Solomon, and S. D. Wilcock, The three-dimensional seismic velocity structure of the East Pacific Rise near latitude 9°30′N, *Nature*, *347*, 639–645, 1990.

Van Avendonk, H. J. A., A. J. Harding, J. A. Orcutt, and J. S. McClain, A two-dimensional tomographic study of the Clipperton transform fault area, *J. Geophys. Res.*, *103*, 17,885–17,899, 1998.

Vera, E. E., J. C. Mutter, P. Buhl, J. A. Orcutt, A. J. Harding, M. E. Kappus, R. S. Detrick, and T. M. Brocher, The structure of 0-to 0.2-m.y.-old oceanic crust at 9°N on the East Pacific Rise from expanding spread profiles, *J. Geophys. Res.*, *95*, 15,529–15,556, 1990.

———————
S. Bazin, Laboratoire de Géosciences Marines, Institut de Physique du Globe de Paris, 4, place Jussieu, case 89, 75252 Paris Cedex 05, France. (bazin@ipgp.jussieu.fr)